

Comparison of techniques to reconstruct VHE gamma-ray showers from multiple stereoscopic Cherenkov images

W. Hofmann*, I. Jung, A. Konopelko, H. Krawczynski,
H. Lampeitl G. Pühlhofer

*Max-Planck-Institut für Kernphysik, P.O. Box 103980, D-69029 Heidelberg,
Germany*

**Corresponding author (Werner.Hofmann@mpi-hd.mpg.de
Fax +49 6221 516 603, Phone +49 6221 516 330)*

Abstract

For air showers observed simultaneously by more than two imaging atmospheric Cherenkov telescopes, the shower geometry is overconstrained by the images and image information should be combined taking into account the quality of the images. Different algorithms are discussed and tested experimentally using data obtained from observations of Mkn 501 with the HEGRA IACT system. Most of these algorithms provide an estimate of the accuracy of the reconstruction of shower geometry on an event-by-event basis, allowing, e.g., to select higher-quality subsamples for precision measurements.

1 Introduction

The HEGRA system [1–3] of imaging atmospheric Cherenkov telescopes (IACTs) is the first installation employing the stereoscopic observation of air showers with multiple Cherenkov telescopes on a routine basis. Compared to individual telescopes, IACT stereoscopy provides an improved reconstruction of shower parameters and better background rejection (see, e.g., [4]). Major new instruments for VHE gamma-ray astronomy now in the construction phase – such as VERITAS [5] and HESS [6] – are based on the concept of IACT stereoscopy, with frequently half a dozen or more telescopes observing the same shower from different viewing angles.

In Cherenkov telescopes [7], the Cherenkov light emitted by shower particles is imaged onto a “camera” in the focal plane of a large reflector, generating an elongated, roughly elliptical image. The major axis of the image represents the image of the shower axis. Therefore, the

major axis of the image points towards the image of the source on one side, and to the point where the shower axis intersects the plane of the telescope dish on the other side (Fig. 1). If a shower is observed by a stereoscopic system of two Cherenkov telescopes, its direction (i.e., the image of the source) can be determined by superimposing the two images and intersecting their major axes. Similarly, the core location is obtained by intersecting the image axes, starting from the locations of the two telescopes (assuming that all telescope dishes are in a common plane). Thus, the four parameters describing the major axes of the two images can be used to determine the four parameters describing the shower geometry - a direction in space and an impact point in a reference plane. It may be worth noting that the stereoscopic reconstruction of air showers makes the single (trivial) assumption than on average Cherenkov images are symmetric with respect to the (image of the) shower axis.

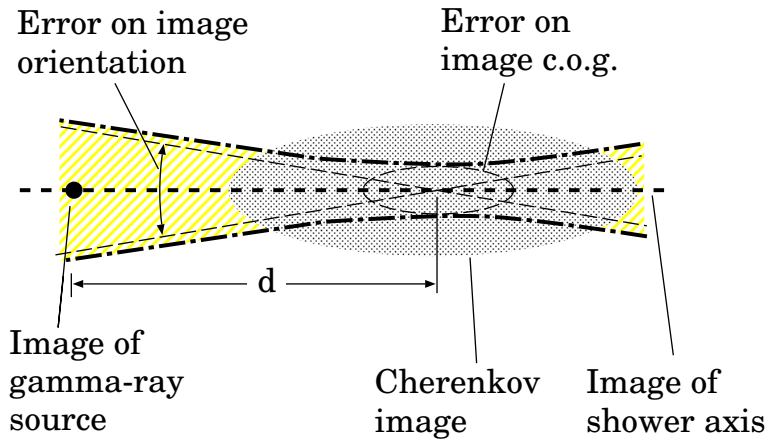


Fig. 1. Cherenkov image of a gamma-ray shower and its interpretation. The major axis of the image approximates the image of the shower axis; the image of the gamma-ray source is located on the image of the shower axis. Due to fluctuations in the shower development and in the imaging process, the center of gravity (c.o.g.) of the image can be displaced from the shower axis, and also the orientation of the image can deviate. These errors are indicated as an error ellipse for the image c.o.g., and an error on the image orientation. Taking into account these errors, the image of the source is constrained to the region between the dashed-dotted lines. Since with a simple elliptical parameterization there is a head-tail ambiguity of the image, the source can be located on either side of the image. The shape of the image, in particular its ellipticity, can be used to estimate the shower impact parameter relative to the telescope and hence the distance d between the image of the source and the c.o.g. of the Cherenkov image.

If a shower is observed by more than two telescopes, the shower geometry is overconstrained and some kind of suitable averaging or fitting procedure is required to extract optimum shower parameters from the information obtained from the different views. Particularly crucial is the case where the quality of the information provided by the different telescopes differs significantly, e.g. because one telescope is well within the light pool and sees a large intensity of Cherenkov light, whereas a distant telescope may see barely enough light to provide a meaningful image. Ideally, the reconstruction algorithm should take this difference in image quality into account. This paper reviews a number of different algorithms and describes tests of their performance based on the large sample of gamma rays [3] collected with the HEGRA IACT system during the 1997 outburst of Mkn 501.

2 Techniques to reconstruct the shower geometry

To reconstruct shower parameters from the telescope images, two alternative approaches can be followed:

Using image parameters. Images provided by the different telescopes are analyzed individually, and their key features are summarized in a small number of parameters (usually the well-known Hillas parameters). Shower parameters are derived on the basis of these image parameters.

Using the full image information. A global optimization procedure is applied to derive the shower parameters directly from the amplitudes measured in the individual pixels of all cameras. An example of such techniques are global fits, where parameterized shower images or image templates are matched to the images observed in the different telescopes [8,9].

In this paper, we will concentrate primarily on methods of the first type. They are easier to implement, and usually require significantly less processing time. Often, analytical solutions for the shower parameters can be derived, and one does not have to worry about issues which arise in numerical optimization procedures, such as the choice of proper starting values and the convergence to the global optimum. For completeness and to serve as a reference, also results based a technique of the second type will be given.

We will discuss seven different algorithms, six based on the Hillas image parameters and one based on a global fit to pixel amplitudes.

Algorithm 1. For all pairs of telescopes, the image axes, derived using the Hillas parameterization, are intersected. In case of N telescope images, the resulting $N(N - 1)/2$ intersection points are averaged, weighted with the sine of the angle between the image axes, to take into account that image pairs with a large stereo angle provide the most precise determination of the shower axis. Similarly, the core location can be obtained by intersecting the image axes, starting from the telescope locations. This technique is used, e.g., for all published results from the HEGRA IACT system. It is illustrated in Fig. 2(a).

Algorithm 2. A drawback of Algorithm 1 is that differences in the quality of the images in the different telescopes are not taken into account. The algorithm can be improved by determining the uncertainty in the determination of the image c.o.g. and in the direction of the image axis, and by taking the resulting errors (see Fig. 1) into account when intersecting the image axes, see Fig. 2(b). For N intersecting lines with fixed error bands, the optimum solution can be derived analytically. Since the width of the error band associated with each image depends on the distance d to the image c.o.g., one needs to iterate, but the result is stable after two iterations. This method also provides errors on the shower parameters.

Algorithm 3. The image shape contains information on the distance d (Fig. 1) between the image c.o.g. and the image of the source. In particular, the ratio of image *width* over image *length* can serve as a measure for d (see also [10]). Smaller *width/length* implies large impact distance and large d . Together with a suitable error estimate for d , the location, orientation and shape of each image constrains the image of the source to two elliptical regions on both

sides of the image (reflecting the left-right ambiguity inherent in the parameterization of shower images), see Fig. 2(c). For two or more images, these error ellipses can be combined analytically to yield the optimum shower direction and its errors. An analogous method determines the core location.

Algorithm 4. Algorithms 1,2,3 determine independently the shower direction and the core location. Since the measurement of the image orientation is used both in the determination of the shower direction and of the shower core, a combined determination of core and direction should yield improved results. Technically, for a given shower geometry, the predicted image center lines are calculated, and a χ^2 is defined measuring the agreement of the observed image and its orientation with this prediction. Shower geometry is chosen to minimize the sum of χ^2 over telescope images. This method is illustrated in Fig. 2(d).

Algorithm 5. Algorithm 4 can be augmented to include the estimate of d from the *width/length*-ratio (see Algorithm 3), by adding corresponding terms to the χ^2 .

Algorithm 6. Similar to algorithm 4, this algorithm – proposed by Hillas [11] – calculates the image axes for a given shower geometry, and varies the shower parameters such as to minimize the sum of the squared distances of pixels to the axes, weighted with the pixel amplitudes. This technique is analogous to the determination of the image axis for single images, except that the weighted sum of pixel distances is minimized for the entire set of images together, rather than for single images ¹.

Algorithm 7. This last algorithms makes use of the full image information, by comparing the measured images with parameterizations of shower images, considering the shower geometry, the energy and the height of the shower maximum as free parameters which are chosen to minimize the χ^2 describing the agreement between model and data. On the basis of Monte-Carlo simulations, the technique was discussed in [8]; a similar method was presented in [9]. The method used here differs from [8] in a different choice of weights, which result in improved convergence.

In our implementation, Algorithms 1,2 and 3 use analytic expressions (with one iteration in case of Algorithm 3), whereas Algorithms 4 through 7 are based on numerical minimization procedures.

3 Data sample

To test the different algorithms and to experimentally determine the directional resolution achieved with each algorithm, data collected with the HEGRA IACT system during the 1997 outburst of Mkn 501 were used. In the HEGRA IACT system is located on the site of the Observatorio del Roque de las Muchachos on the Canary Island of La Palma at 2200 m asl. In 1997, the IACT system comprised four telescopes, located in the center and at three sides of a

¹ At first glance, Algorithm 6 may appear as an algorithm using the full pixel information rather than the image parameters. However, given the Hillas image parameters, equivalent to the moments of inertia of the image with respect to the major and minor axis, one can easily calculate the second moment with respect to an arbitrary axis.

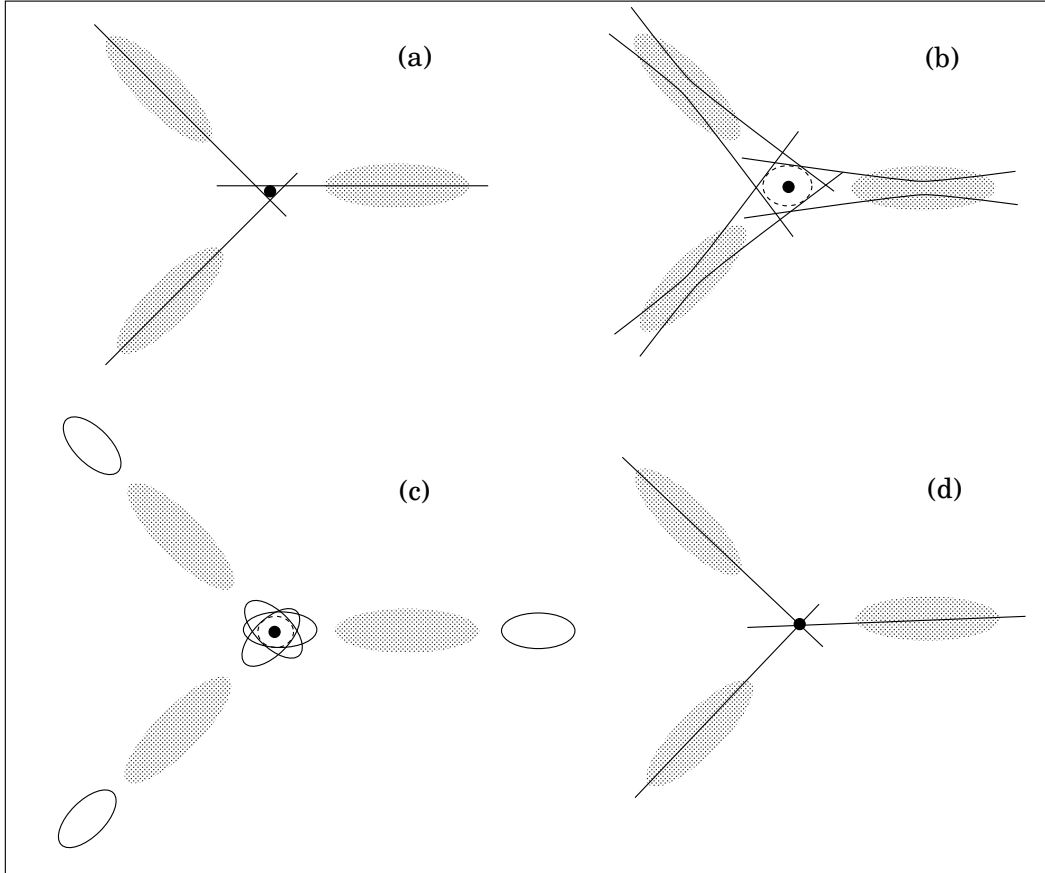


Fig. 2. Illustration of different techniques to determine the shower direction from multiple Cherenkov images. (a) Intersecting pairs of image axes, followed by an averaging over intersection points. (b) Intersecting image axes taking into account the errors on image location and image orientation, resulting in an error ellipse for the image of the source. (c) Using in addition the *width/length*-ratio to constrain the source image to two regions on either side of an image. (d) Optimizing the shower geometry such that the predicted image axes best match the observed images.

square with roughly 100 m side length. A fifth telescope at the remaining corner was integrated into the system in 1998. The telescopes are identical, equipped with 8.5 m² mirrors with 5 m focal length, and with 271-pixel cameras with a diameter of the field of view of 4.3°, and an equivalent pixel size of 0.25°. Detailed about the hardware and the data analysis can be found in [1–3,12].

The trigger condition for individual telescopes requires a coincidence of two pixels above a threshold of 10 photoelectrons (before June ‘97) or 8 photoelectrons (after June ‘97). For typical gamma-ray images, cameras trigger once the image has more than about 40 photoelectrons. The HEGRA IACT system as a whole is triggered and data are recorded whenever at least two telescopes trigger in coincidence (see [2] for details on the trigger system).

In the design of the HEGRA cameras and their electronics, an important aspect was that one wanted to read out not only those telescopes which had triggered, but also the remaining telescopes, which will shower fainter, but frequently still usable images. Camera signals are

digitized continuously by 120 MHz Flash-ADCs and are stored in a 34 μs ring buffer. A coincidence trigger of at least two telescopes is generated with a delay of 1 to 2 μs ; After such a trigger, the readout system addresses the relevant locations in the Flash-ADC memory and extracts the signals.

In 1997, Mkn 501 was observed in the so-called wobble mode, with the source offset by 0.5° in declination from the optical axis of the telescopes. The offset alternated every 20 min. A region offset by the same amount, but in the opposite direction, is used as a control region and for background subtraction.

The analysis is based on data taken during three new-moon periods, where the gamma-ray flux from Mkn 501 was particularly high. Only data at small zenith angles, below 20° , are included; these showers behave essentially like “ideal” vertical showers, at least as far as the angular reconstruction is concerned. The usual selections concerning data quality were applied, see [3]. In total, the sample comprises 100748 events within 0.5° from the source, and 80878 events in the equivalent off-source region.

Images were flat-fielded, and corrections for pointing errors of the telescopes were applied [13]. Image parameters were determined by selecting “image pixels” as those pixels which either have a signal of 6 or more photoelectrons, or which have a signal of at least 3 photoelectrons and are adjacent to a pixel with 6 or more photoelectrons.

4 Errors assigned to image parameters, and angular resolution

Some of the algorithms discussed above require errors on the image parameters as input for the reconstruction of the shower axis. The relevant image parameters are the coordinates (x, y) of the center of gravity of the images, and the direction θ of the major axis of the image. To parameterize the errors on the center of gravity, it is more convenient to use a coordinate system where axes (u, v) are defined by the major (u) and minor (v) axes of the image. In this system, the errors on u , v , and on the orientation θ of the image should be essentially uncorrelated. The errors (in units of degr.) were parameterized on the basis of Monte-Carlo simulations [14]:

$$\Delta v = \left\{ \frac{0.03}{A} + 0.009^2 \right\}^{\frac{1}{2}} f(w) \quad , \quad f(w) = \begin{cases} 1 & \text{if } w < 0.08 \\ w/0.08 & \text{if } w \geq 0.08 \end{cases}$$

and

$$\Delta\theta = \left\{ \left(\frac{600}{A} \right)^{1.5} + 1.1^2 \right\}^{\frac{1}{2}} + 45 \left(\frac{w}{l} - 0.2 \right)^2$$

Here, A denotes the number of photoelectrons in the image (*size*), w the image *width* and l the *length*. The error in u is not very relevant as long as the major axis of the image points more or less towards the source; $\Delta u = 2\Delta v$ was used.

As a first check to see if these errors describe the uncertainties in the real data, the distribution in *miss* was plotted for individual telescopes of the (background subtracted) Mkn 501 gamma-ray sample, with the (signed) *miss* parameter normalized to the expected error. The *miss* parameter describes the distance between the image axis and the point on the camera which corresponds to the image of the source. The error on *miss* is $\Delta_{miss}^2 = d^2 \Delta\theta^2 + \Delta v^2$. For typical values of $d \approx 1^\circ$ the $\Delta\theta$ term gives the dominant contribution. The normalized *miss* distribution has an rms width of 1.06, and its central part is well described by a Gaussian with a width of 0.90, indicating both that the errors estimated are accurate within 10%, and that alignment errors of the telescopes are small on the scale of the resolution.

To verify that also errors on the shower direction can be reliably calculated by propagating the errors on the image parameters, events were reconstructed with Algorithm 2 and those events were selected where the predicted error on the shower direction was less than 0.04° (Fig. 3(a)). For these events, the distribution in the difference between the reconstructed shower direction and the source, Mkn 501, was plotted (Fig. 3(b)), projected onto two orthogonal axes. Indeed, for this subsample of events, a (projected) angular resolution of 0.037° is obtained, confirming the validity of the approach to estimate the errors, by treating the image parameters obtained by the different telescopes as independent measurements. Here and in the following, ‘angular resolution’ refers to the width of the angular distribution of shower axes in a projection. If angular resolution is defined as the half opening angle of a cone in space, which contains 68% of the events, the numerical values are a factor 1.5 larger (assuming a Gaussian distribution in the errors).

Fig. 3(c) finally shows the measured angular resolution as a function of the predicted resolution, demonstrating good agreement except for the tail of events with very large predicted errors ($> 0.2^\circ$), where the measured angular resolution is slightly better than expected (most likely due to imperfections in the parameterizations of the errors). Hence, already with the extremely simple and fast Algorithm 2 one can reliably reject events with poorly reconstructed showers, which is important, e.g., for the determination of energy spectra.

In addition to errors on the image parameters, Algorithms 3 and 5 require an estimate of d based on the image shape; we used the empirical relations

$$d = 1.4 - 1.25 \frac{w}{l} \quad , \quad \Delta d = \max \left(\frac{2.5}{\sqrt{A}} , 0.15 \right)$$

5 Comparison of reconstruction techniques

The angular resolutions obtained with the seven algorithms described above are summarized in Fig. 4, for three characteristic data samples chosen to emphasize the specific features on the algorithms:

2-Telescope events (full squares). In these events, exactly two telescopes have triggered, and only these two telescopes are used for the reconstruction. The 2-Telescope sample serves

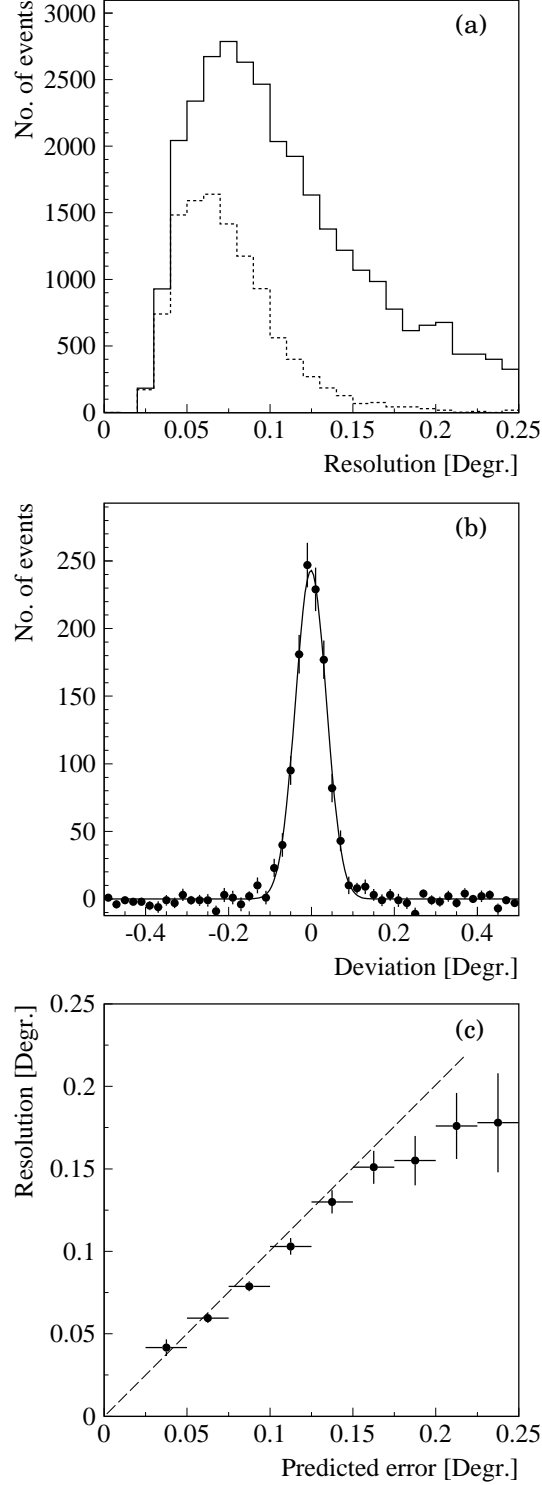


Fig. 3. (a) Predicted uncertainty in the measurement of the (projected) direction of the shower axis, for events with at least two triggered telescopes (full lines) and for events where all four telescopes triggered (dashed). Only triggered telescopes are used in the reconstruction. (b) Deviation between the measured shower axis and the direction to Mkn 501 for events with a predicted angular error of less than 0.04° , after statistical subtraction of the background. The curve represents a Gaussian fit with a width of 0.037° . (c) Experimental angular resolution (in projections), determined using a Gaussian fit, as a function of the predicted error of the measurement.

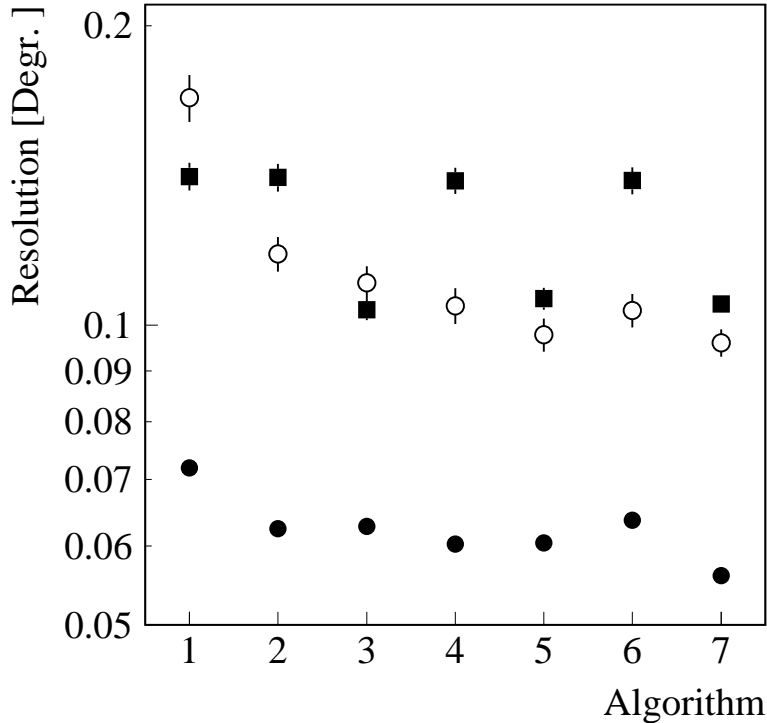


Fig. 4. Angular resolution obtained from the Mkn 501 data with the various algorithms, for different data samples and reconstruction modes. Full squares: events with exactly two triggered telescopes, using only these two telescopes; open circles: events with exactly two triggered telescopes, using images in all four telescopes; full circles: events where all four telescopes triggered and all images are used.

primarily to verify that all algorithms work properly; unless additional shape information is used (such as in Algorithms 3, 5, and 7), all algorithms should give identical results if only two images are used in the reconstruction ².

2+2-Telescope events (open circles). In these events, exactly two telescopes have triggered, but images in the other two untriggered telescopes are included in the reconstruction. These events represent a particular challenge to reconstruction algorithms, since they combine images of very different quality. Triggered images contain a mean number of about 150 photoelectrons, compared to about 30 photoelectrons in images which did not trigger.

4-Telescope events (full circles). In these events, all four telescopes have triggered and are used in the reconstruction. This class of events will obviously provide the best angular resolution.

For the 2-Telescope sample (full squares in Fig. 4), Algorithms 1, 2, 4 and 6 do indeed provide the identical angular resolution. Algorithms 3, 5 and 7 – which add shape information – give significantly improved resolution. This improvement can be traced to events with small stereo

² It should be noted that there is a big difference between the 2-Telescope sample, where exactly two of the four telescopes triggered, and samples (“2/x”) where two telescopes are used for the reconstruction, regardless of the state of the other two. The 2-Telescope sample selects events which either have energies near the trigger threshold, or which have quite distant cores. A 2/x-Telescope sample yields for Algorithm 2 a resolution of about 0.10°, compared to the 0.14° for the 2-Telescope sample – see below.

angles, i.e. with shower cores along the line connecting the two telescopes; for such events, the purely geometrical reconstruction fails and the otherwise relatively poor shape information helps to stabilize the reconstruction.

Adding now in the reconstruction the faint images of the other two telescopes, which did not trigger – the 2+2-Telescope sample (open circles) – one mixes images of rather different quality. If all images are combined with equal weight, as in Algorithm 1, the faint images hurt the resolution; the resulting resolution is worse than if only the two triggered telescopes are used. In all other algorithms, the faint images weigh less than the good images, either because explicitly larger errors on the image parameters are assigned (Algorithms 2-5), or because the effect of the images is weighted with the number of photoelectrons they contain (Algorithms 6,7). These algorithms improve the angular resolution by about 20% to 30% compared to the 2-Telescope sample. Little is gained by adding the shape information via the $d(w/l)$ relation; with four views there is always at least one reasonably large stereo angle.

In many respects, the 4-Telescope sample (full circles) is less critical than the 2+2-Telescope sample, since the differences between the quality of the four images are not nearly as big. Hence, it is no surprise that the variation between algorithms is smaller, ranging from a resolution of 0.072° for the worst case (Algorithm 1) to 0.056° for the best case (Algorithm 7).

One may wonder why the joint fits of the shower direction and of the core location (Algorithms 4, 5, 6) do not provide significant improvements. The explanation is relatively simple, and is illustrated in Fig. 5. The geometrical figure describing the determination of the direction (Fig. 5(a)) and the figure describing the determination of the core (Fig. 5(b)) are essentially scaled versions of each other, since the *distance* parameter d of the image is approximately proportional to the distance r from the telescope to the core location. The main difference is that in the determination of the shower direction, the error on the position of the image c.o.g. enters in addition to the error on the image orientation; in the core determination, only the latter matters. Since the error on the c.o.g. is usually of little relevance compared to the error on the orientation, the joint fit does not add additional constraints. Indeed, one finds that in Algorithm 2, the χ^2 describing how well the telescopes match in the determination of the shower direction, and the χ^2 of the core determination are highly correlated (Fig. 5(c)).

Fitting the full image information (Algorithm 7) results in only very modest improvements compared to the simpler Algorithms 2 - 6. At least with the pixel size of 0.25° of the HEGRA cameras, the Hillas image parameters seem to very efficiently capture the essence of the information contained in the images.

6 Dependence of the angular resolution on the number of telescopes used in the reconstruction

An interesting question is how the angular resolution depends on the number of telescopes N_{tel} used in the reconstruction. If the individual images can be considered as independent, the

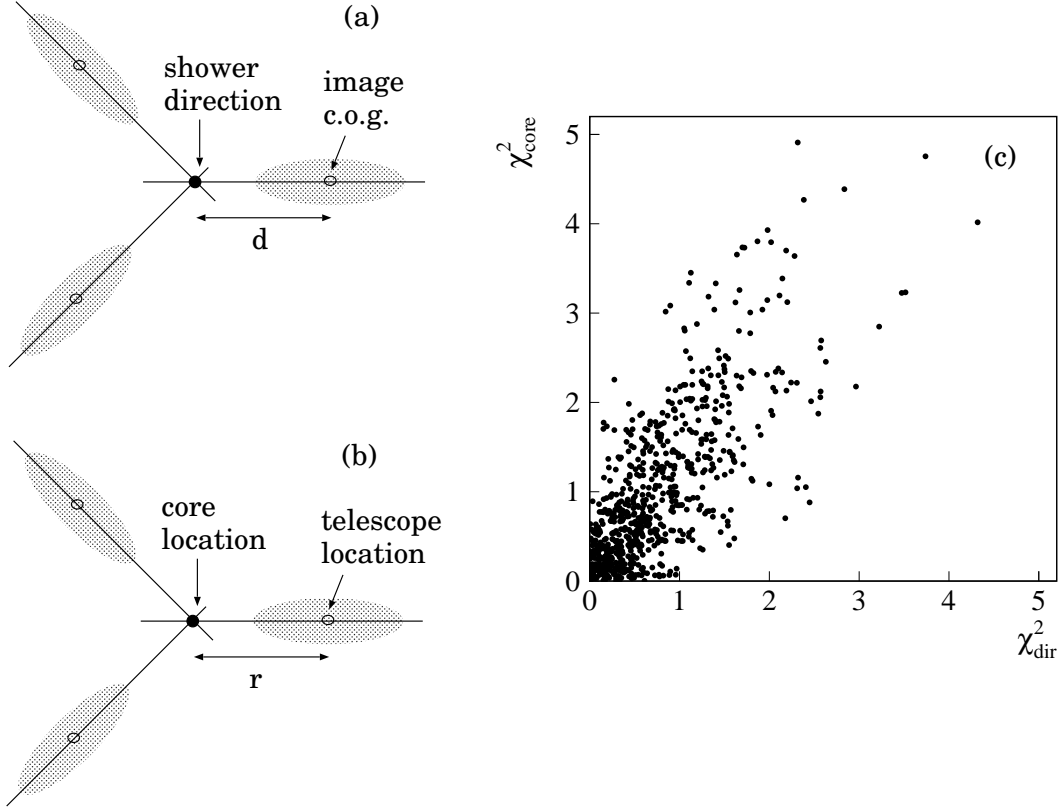


Fig. 5. (a) Reconstruction of the shower direction, by intersecting the image axes, starting from the image c.o.g. (b) Reconstruction of the shower core by intersecting the image axes, starting from the telescope locations. (c) χ^2 describing the consistency in the determination of shower cores in overconstrained events, vs. χ^2 describing the consistency of the determination of the shower direction, for background-subtracted gamma-ray events from Mkn 501.

resolution should improve like $1/\sqrt{N_{\text{tel}}}$. However, at some point shower fluctuations will start to dominate the resolution.

As mentioned above, to address this issue one cannot simply use the event samples where exactly 2, 3 or 4 telescopes have triggered, since the 2-telescope sample is biased towards low-energy or distant showers, whereas in the 4-telescope sample central high-energy events are enhanced. To start from identical event samples and to avoid a “trigger bias”, the investigation was based on the 4-telescope sample, but only a subset of telescopes was used to reconstruct the shower. The resulting resolutions are illustrated in Fig. 4(a), for Algorithms 2 and 3. (Note that Algorithm 3 can reconstruct the shower direction from a single image, apart from the head-tail ambiguity.) Except for the minimum number of telescopes – 1 for Algorithm 3 and 2 for Algorithm 2 – data are consistent with a $1/\sqrt{N_{\text{tel}}}$ -dependence.

The issue was further explored on the basis of Monte-Carlo simulations for the HESS telescope system [15]. These simulations used an array of 589 telescopes, arranged as a square grid of 31 x 19 telescopes, spaced 33.3 m. In the analysis, arbitrary subsets of telescopes can be selected. The sets studied here include a set with all telescopes turned on, a set where every other telescope is active, and sets with telescopes on square grids with an effective spacing of

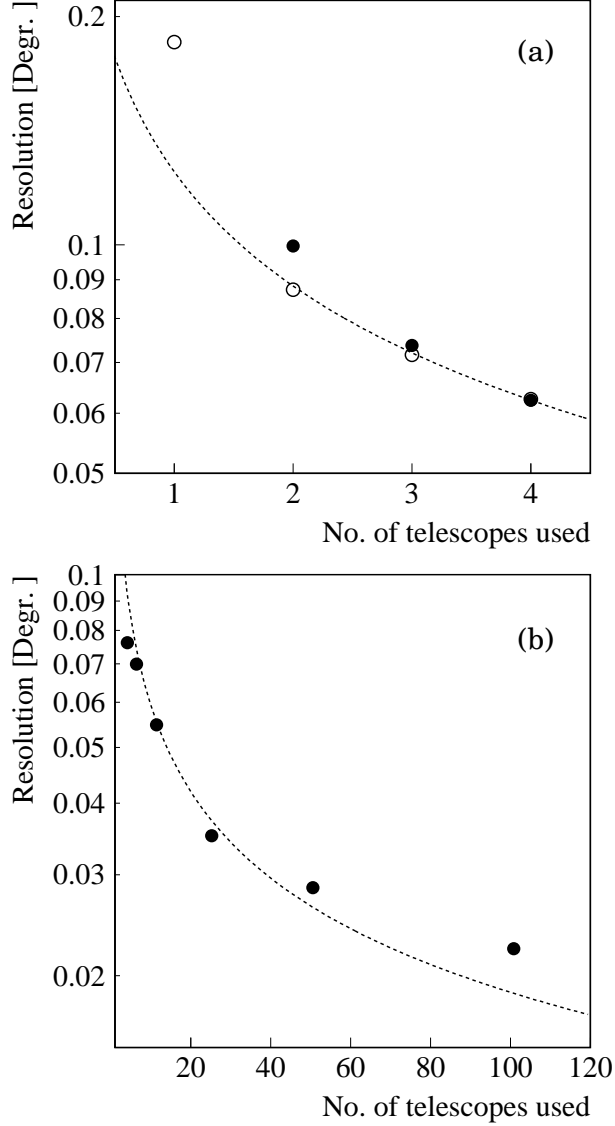


Fig. 6. (a) Angular resolution obtained from the Mkn 501 data with Algorithm 2 (full circles) and Algorithm 3 (open circles), for events where all four telescopes triggered, but only a (random) subset of telescopes is used in the reconstruction. The curve illustrates a $1/\sqrt{N_{tel}}$ -dependence. (b) Angular resolution obtained in Monte-Carlo studies using an array of telescopes, as a function of the average number of telescopes used in the reconstruction. Shower energies range from 0.5 TeV to 1 TeV. The curve illustrates a $1/\sqrt{N_{tel}}$ -dependence. (The telescope characteristics differ from those of the HEGRA telescopes, and the resolutions cannot be compared directly.)

67 m, 100 m, 133 m, and 167 m. Only showers well contained within the array were considered. Fig. 6(b) shows the resulting angular resolution as a function of the mean number of telescopes used in the reconstruction. The $1/\sqrt{N_{tel}}$ -dependence of the resolution holds up to about 50 telescopes used per event, and resolutions better than 0.03° . For even higher telescope numbers, the dependence appears to flatten somewhat.

7 Concluding remarks

The main conclusions from these studies of different algorithms for the stereoscopic reconstruction of multi-telescope IACT events are:

- By assigning and properly propagating errors of the image parameters, reliable error estimates for the shower direction can be obtained. It is possible to select subsamples with improved angular resolution – less than 0.05° , e.g. – for special purposes, such as to study the size of the source, or to exclude poorly reconstructed events.
- In particular when combining multiple and partly redundant images of rather different quality, the reconstruction algorithm must properly account for these differences.
- Using image shape information to constrain the direction of the shower axis helps in the case of 2-telescope events with small stereo angles; for events with more than two telescopes, the improvement is small.
- Compared to the simple, robust and fast Algorithms 2 and 3, the more ‘fancy’ Algorithms 4, 5 and 6 as well as the rather sophisticated image fitting procedure of algorithm 7 give only modest improvements. For most practical purposes; Algorithms 2 or 3 may represent the simplest and best choice.

Of course, these conclusions hold primarily for the HEGRA Cherenkov telescopes. To which extent they can be applied to other IACT systems depends on the degree of similarity in the trigger concept and the layout of the cameras.

Acknowledgements

The support of the HEGRA experiment by the German Ministry for Research and Technology BMBF and by the Spanish Research Council CYCIT is acknowledged. We are grateful to the Instituto de Astrofísica de Canarias for the use of the site and for providing excellent working conditions. We thank the other members of the HEGRA CT group, who participated in the construction, installation, and operation of the telescopes. We gratefully acknowledge the technical support staff of Heidelberg, Kiel, Munich, and Yerevan.

References

- [1] A. Daum et al., *Astropart. Phys.* 8 (1997) 1.
- [2] N. Bulian et al., *Astropart. Phys.* 8 (1998) 223.
- [3] F. Aharonian et al., *Astron. Astrophys.* 342 (1999) 69.
- [4] F. Aharonian et al., *Astropart. Phys.* 6 (1997) 343, 369.

- [5] Veritas Letter of Intent, T.C. Weekes et al. (1997).
- [6] HESS Letter of Intent, F. Aharonian et al. (1997).
- [7] T.C. Weekes, *Space Science Rev.* 75 (1996) 1; M. F. Cawley and T.C. Weekes, *Experimental Astronomy* 6 (1996) 7.
- [8] M. Ulrich et al., *J. Phys. G* 24 (1998) 883.
- [9] S. Le Bohec et al., *Nucl. Instr. Meth.* A416 (1998) 425.
- [10] C.W. Akerlof et al., *Astroph. J.* 377 (1991) L97; J.H. Buckley et al., *Astron. Astrophys.* 329 (1998) 639; V. Connaughton et al., *Astropart. Phys.* 8 (1998) 179.
- [11] M. Hillas, talk at the Workshop on TeV Gamma-Ray Astronomy with Systems of Cherenkov Telescopes, Ringberg Castle (1996).
- [12] G. Hermann, *Proceedings of the Int. Workshop "Towards a Major Atmospheric Cherenkov Detector IV"*, Padua, (1995), M. Cresti (Ed.), p. 396.
- [13] G. Pühlhofer et al., *Astropart. Phys.* 8 (1997) 101.
- [14] A. Konopelko et al., *Astropart. Phys.*, in print, and astro-ph/9901199.
- [15] A. Konopelko, *Astropart. Phys.*, in print, and astro-ph/9901365.